AAIA 94-2516

Measurement of Scramjet Thrust in Shock Tunnels

R.J. Stalker, J.M. Simmons, A. Paull, D.J. Mee
Department of Mechanical Engineering
The University of Queensland
Brisbane, Australia

18th AIAA Aerospace Ground Testing Conference
June 20-23, 1994 / Colorado Springs, CO

MEASUREMENT OF SCRAMJET THRUST IN SHOCK TUNNELS

R.J. Stalker*, J.M. Simmons†, A. Paull‡, D.J. Mee§
Department of Mechanical Engineering, The University of Queensland
Brisbane, Australia

Abstract

By using results obtained in tests on supersonic combustion of hydrogen in air, the conditions governing model size and operating pressure levels for shock tunnel experiments on models of flight vehicles with scramjet propulsion are established. It is seen that large models are required. The development of the stress wave force balance is then described, and its use as a method of measuring thrust/drag on such models is discussed. Test results on a simple, fully integrated scramjet model, with intakes, combustion chambers, thrust surfaces and exterior surfaces, using a 13% silane 87% hydrogen fuel mixture, showed that a steady state with thrust generation could be achieved within the shock tunnel test time, and the thrust could be measured. Results are presented for a range of stagnation enthalpies, and show that the scramjet model produces net positive thrust at velocities up to 2.4 km/sec.

Nomenclature

D	length of combustion chamber
H_0	test section stagnation enthalpy
L	overall length of model
M_c	Mach number of entrance to combustion chamber
P	pressure at entrance to combustion chamber
P_0	shock tunnel nozzle reservoir pressure
T	temperature at entrance to combustion chamber
V	test section velocity
ΔI_{SP}	specific impulse increment
γ	ratio of specific heats in test gas
ϕ	fuel equivalence ratio

1. Introduction

The scramjet offers a method of propulsion which, in principle, is able to operate up to any flight speed and, in fact, seems likely to be effective for flight speeds approaching 5 km/sec. A considerable amount of research has been done on the components of scramjets, with the inlet, the combustion chamber and the thrust nozzle all receiving attention. The components have also been coupled together, to make a complete scramjet engine, and various forms of this type of engine have been subjected to experimental scrutiny[1,2].

However, the ultimate test of a propulsive device is its performance when installed in an appropriate flight vehicle. This is particularly true of the scramjet, where the need to integrate the aerodynamics of the vehicle and the operation of the engine is particularly acute. Where circumstances prevent extensive experimentation with a series of flight vehicles, the next best thing is experimentation in ground facilities with models of the engines installed in models of the vehicles. Notwithstanding the desirability, experimentation of this type has not been reported for the hydrogen fuelled scramjet, at least in the open literature, and the purpose of the present paper is to discuss experiments which indicate that this is possible.

At speeds above about 2.5 km/sec, impulse facilities offer the only means of producing wind tunnel type flows for aerodynamic testing. Chief among these is the shock tunnel which, in its various forms, is able to achieve speeds ranging up to orbital velocity. Therefore, because it covers the range of speeds likely to be associated with scramjet operation, the discussion is centred on experiments in a shock tunnel.

---

*Professor of Space Engineering

†Professor & Dean of Engineering

‡Research Fellow

§Lecturer

It can be seen that ΔI_{SP} in Figure 3 exhibits a maximum at approximately 1000 K. This was a general feature of the experiments, and it was possible to plot the points at which a given level of maximum specific impulse increment was achieved on a graph of P Vs D, as in Figure 4. The data for this figure was obtained at equivalence ratios of 1.0 ± 0.1. Two levels of maximum specific impulse increment are considered, and it can be seen that there is a factor of two or three difference in the pressures needed to achieve the respective levels. (A question mark adjacent to one point indicates that experimental evidence suggests that the same ΔI_{SP} may have been obtained at a lower value of P). Two curves are shown, which represent an attempt to correlate the results according to the rule PD = constant. It can be seen that this is only partly successful, and that effects appear to be present which modify this rule. For example, the two experimental points at D = 575 mm were obtained at a combustor inlet Mach number of 4.5, whereas the other results were obtained at Mach numbers of 3.5 ± 0.2, indicating that combustor Mach number may be influencing the results. Notwithstanding this, it will be assumed that the rule PD = constant provides an order of magnitude estimate of the required combustion chamber length and pressure to yield a substantial specific impulse increment.

Also, the fact that the peak specific impulse increment occurred at a combustor inlet temperature of approximately 1000 K implies that the combustor inlet Mach number would be approximately one half of the Mach number achieved by a flight vehicle in which the combustor was installed or, in a shock tunnel, where the flight Mach number may not be simulated, the combustion Mach number would be approximately 1.5 times the free stream velocity in km/sec.

(b) Model Size and Shock Tunnel Requirements

From the results above, it is possible to make approximate estimates of the model size and the associated shock tunnel requirements pertaining to test of a scramjet propelled vehicle configuration.

The relation between model size and combustion chamber length depends, of course, on the design of the vehicle. However, the fact that such a vehicle would require a small forebody angle, and a not-so-large afterbody angle making a thrust surface, implies that the overall vehicle length may be expected to be an order of magnitude greater than the combustion chamber length. Therefore it is assumed that

$$L \approx 10D \qquad (1)$$

Now, the combustion chamber inlet pressure is determined by the combustion chamber inlet Mach number M_c and the nozzle reservoir pressure of the shock tunnel, P_0. Assuming isentropic compression in the scramjet intake, and a perfect gas,

$$P = P_0\left(1 + \frac{\gamma-1}{2}M_c^2\right)^{-\gamma/(\gamma-1)}, \qquad (2)$$

where γ is the ratio of specific heats. It is assumed that $\gamma = 1.3$. For a combustion chamber which yields a specific impulse increment of 1500 sec, the upper curve in Figure 4 applies approximately, and so

$$PD = 0.3 \text{ m.atm.} \qquad (3)$$

Thus, eqns (1), (2) and (3) enable the length of the model corresponding to given values of M_c and P_0 to be obtained.

Values so obtained are presented in Figure 5, for three values of the shock tunnel nozzle reservoir pressure. The curves show the extreme difficulty associated with testing at high combustor inlet Mach numbers. If a model length of 5 m and a nozzle reservoir pressure of 2000 atm. is taken as representing the practical limits of modern shock tunnel technology, then it can be seen that testing will be limited to a combustor inlet Mach number of 6, corresponding to a flight velocity of 4 km/sec. Whilst it should be noted that some rather sweeping approximations have been made in obtaining Figure 5, and therefore the values of L may, in practice, vary somewhat from those presented in the figure, the strong dependence on M_c implies that the limit will be close to the predicted value.

Thus, Figure 5 shows that the maximum combustion inlet Mach number in any shock facility depends on the length of the model which can be accommodated. In the absence of extensive regions of separated flow, the working rule for shock tunnels is that the length of the slug of test gas passing through the tests section should be at least 3L. Assuming that the test section size imposes no constraints on the model length, it follows that the maximum value of L is determined by the test time, which therefore determines the maximum combustion inlet Mach number, and hence the maximum flight velocity at which scramjet propulsion of a flight vehicle

The paper begins by considering tests on a scramjet combustor and thrust nozzle combination. These tests are used to define the approximate overall size of a model incorporating a scramjet, and this is seen to make severe demands on conventional techniques of measuring force on the model. The development of a new technique is described, particularly as it applies to the measurement of drag or thrust. This technique is then used to measure the thrust/drag of a non-lifting configuration incorporating scramjets.

2. The Shock Tunnel

The experiments were conducted in the free piston shock tunnel T4 at The University of Queensland, with the exception of some of the early experiments on the combustor/nozzle combination, which were conducted on the free piston shock tunnel T3 at the Australian National University[3]. Since both tunnels are similar in concept, only T4 will be briefly described here.

The layout of T4 is shown in the sketch in Figure 1. The free piston travels along a compression tube 26 m long and 229 mm in diameter to compress and heat the driver gas, before rupturing a diaphragm leading to a shock tube 75 mm in diameter and 10 m long. A shock wave is driven along the shock tube and, upon reaching the end, ruptures a mylar diaphragm and initiates the flow in a contoured, axisymmetric, hypersonic nozzle with a throat diameter of 25 mm and an effective exit diameter of 250 mm. The flow passes through the test section as a free jet.

The reservoir conditions for the nozzle flow are obtained from measurements of the shock speed, the initial pressure in the shock tube and the pressure at the end of the tube following shock reflection. The test section conditions are obtained by computing the expansion of the test gas from the reservoir to the measured value of pitot pressure of the test section.

3. Considerations Regarding Model Size

(a) Combustor/Thrust Nozzle Tests

The experimental configuration used in these tests is shown in Figure 2. Hydrogen fuel was injected into a rectangular duct, with dimensions 25 mm x 50 mm, at the trailing edge of a strut 4.6 mm thick. The strut was mounted to span the 50 mm dimension at the midplane of the duct, and the hydrogen was injected supersonically. Generally, the flow produced by the shock tunnel nozzle passed directly into the duct, so that the combustor effectively operated in the "direct connect" mode. However, in some tests the combustion Mach number was varied by placing a simple intake consisting of a pair of opposing wedges immediately upstream of the duct.

A thrust nozzle was formed by deflecting one of the 50 mm wide walls of the duct as shown. The distance, D, from the point of injection to the beginning of the expansion wave generated by the corner at the beginning of the thrust nozzle was taken as the length of the combustion chamber. This was measured on the centreline of the combustion chamber, and was varied by using inserts in the duct wall immediately upstream of the thrust nozzle. The deflection angle of the thrust surface varied from 15° at a Mach number of 3.5 to 11° at a Mach number of 4.5, so the effective area ratio of the thrust nozzle varied from approximately 12 to 9[4,5]. The thrust was measured by integrating the pressure over the thrust surface and, noting the fuel mass flow through the injector, was converted into a specific impulse.

Using this configuration, the length of combustion chamber required to produce a given specific impulse with a particular combustion chamber inlet pressure, P, could be obtained. It can be argued, of course, that the same specific impulse may be produced with a shorter combustion chamber, and a different fuel injection pattern. However, practical considerations limit the number of injection points, and it seems unlikely that the combustion chamber length would be reduced by more than a factor of two by this approach, even when the combustion is mixing limited. Therefore it is reasonable to take the lengths of the combustion chamber measured in these tests as typical values.

Figure 3 shows the specific impulse increment ΔI_{SP} plotted against combustor inlet temperature for a Mach number of 3.6 ± .1. ΔI_{SP} is obtained by subtracting the thrust with no fuel injection from the thrust with fuel injection to obtain the thrust increment due to fuel injection. Two values of P and of D were chosen, such that the product PD is constant, and can be seen that although P and D individually varied by a factor of three, the thrust increment remained the same over the range of inlet temperatures.

can be simulated in the shock tunnel facility under consideration.

4. Force Measurement in Shock Tunnels - The Stress Wave Balance

(a) Background

The conventional method of measuring forces is to regard the model as lumped mass, and the force balance as a spring system, and to allow a sufficient number of oscillations to come to equilibrium before the force is measured. This is suitable for test times in excess of 10 milliseconds, and therefore cannot be used in much shorter test times of high performance facilities. Therefore a number of fast response techniques have been developed (e.g. ref.6) but although these do offer substantial improvements, they continue to be based on the assumption of a rigid model, and as a consequence, they require that the model be small relative to the tunnel size.

It is seen above that the model may be expected to be of a size such that the flow traverses only a few model lengths during the test time. Furthermore, stress waves induced in the model by the aerodynamic forces propagate at a speed ($3 \rightarrow 5$ km/sec for ordinary model materials such as steel or aluminium) which is comparable with the flow speed, and therefore the model is in an unsteady state of stress during the entire flow period. Thus the model cannot be regarded as rigid, and a method of measuring forces which takes this into account is required.

(b) The Stress Wave Force Balance

Fortunately, the stress waves which are the source of this difficulty can themselves be exploited to measure the force on the model[7]. By placing a strain gauge on the model support sting adjacent to the base of the model, the time history of stress waves passing into the sting is recorded, and this recording can be deconvoluted to yield the force on the model. The relation between the force applied to the model, u(t), and the output of the strain gauge, y(t) can be written as

$$y(t) = \int_0^t g(t-\tau)\, u(\tau)\, d\tau \quad , \qquad (4)$$

where g(t) is an impulse response function expressing the relation between the two.

A simple example of this, shown in Figure 6(a), occurs when the "model" is just an extension of the sting, and the force is applied as a step change in time at the upstream end. In this case the strain gauge records the passage of a stress wave which directly represents the applied load and, in eqn (4), g(t) is simply a delta function. If the model is a cylinder aligned with the flow, as shown in Figure 6, then the application of the force causes a stress wave in the model, which is partially reflected and partially transmitted into the sting at the model-sting junction. The reflected portion traverses the model and returns to the junction to transmit a further stress wave into the sting, and so on. The "ringing" of the stress wave in the model therefore produces a series of transmitted stress waves of decreasing amplitude in the sting, to eventually approach a steady state of stress. The time history of the stress waves in the sting is as shown in Figure 6(b), and g(t) is a series of delta functions.

In either of the above two cases, g(t) is of a sufficiently simple form that the integral in eqn (4) can be readily deconvoluted, and u(t) can be deduced from g(t). However, as the models become more complicated, so does the deconvolution, and it is necessary to use computational techniques.

The impulse response function for a particular model-sting combination can be found either experimentally or by using a dynamic finite element analysis. Tests to date have tended to use the experimentally determined impulse response function, with that determined computationally retained for checking. The experimental determination was assisted by the fact that the model sting was a simple stress wave bar 2 m long, manufactured from 32 mm diameter brass tubing of 1.63 mm wall thickness. This could be readily removed from the shock tunnel with the model attached, and suspended by a fine wire attached to the tip of the model. The wire was then out close to the model to produce a sudden removal of tensile load. This is equivalent to a step-like drag load applied at the tip of the model. The output from strain gauges mounted on the stress wave bar 200 mm from the base of the model then gave the step response for the system, and this response was differentiated with respect to time to yield the experimental impulse response function.

When this technique was first proposed[7] it was applied to the measurement of drag on a short cone, with the results shown in Figure 7. It can be seen that the drag followed the pitot pressure in the test section within 0.2 to 0.3 millisec of

initiation of the flow. In this case the internal stress waves were unimportant, but subsequent measurements on a 425 mm long cone[8], where they were important, showed that they could be taken into account satisfactorily, as shown in Figure 8. Once again it can be seen that the drag follows the pitot pressure within approximately 0.3 millisec. Then measurements of drag of a 5° cone, with varying degrees of nose blunting, showed that the method could accommodate peaks in the load distribution, as represented by a blunt nose[9]. Some results of these tests are shown in Figure 9. Computational modelling indicated that the distribution of force had negligible effect, and only the total drag on the model would be recorded. This was confirmed by the experiments.

During the tests on the blunted cones, it was found that the impulse response function g(t) could be extended in time to take account of stress wave reflections at the downstream end of the stress wave bar. Before this, it was thought that the measurement would be terminated by arrival of these reflected waves at the strain gauge. The extension of time that was made possible by accommodating these reflections was important in scramjet model testing, as will be see below.

With completion of these tests, it was thought that the method was sufficiently developed to apply to thrust/drag measurement of a scramjet model.

It will be observed that in all the tests, the stress wave bar was suspended horizontally in the tunnel by two fine wire threads. Attachment of these threads to the bar did not produce an observable effect on stress wave propagation in the bar.

5. Scramjet Model Thrust/Drag Measurement

(a) The Model

A sketch of the scramjet model and fuel tank is shown in Figure 10. The scramjet centrebody, shown in streamwise section in the figure, consisted of a conical forebody with 9° half angle, a cylindrical section of 51 mm diameter, and an afterbody of 10° half angle. It was partly surrounded by a axisymmetric cowl, which had an internal diameter of 67 mm over the parallel section of the centrebody, and was of 71 mm outside diameter. Filler pieces, which are not shown, divided this parallel section into six constant area combustion chambers, each of which subtended an angle of 26° at the centreline. Fuel was injected through six orifices, each 2 mm in diameter and angled at 30° to the centreline. They were located at the upstream end of the combustion chambers. The filler pieces between the combustion chambers extended upstream in the form of intake compression ramps which processed the flow in the forebody shock layer through two shocks, each of 8° deflection. The leading edges of the cowl were shaped to prevent these shocks spilling from the intake, thus forming a convergent duct leading to the combustion chambers. The radial dimension of this duct was 10 mm.

The fuel supply system is also shown in the figure. The fuel tank was filled before a test, and the supply valve remained closed until the test was initiated. The recoil of the shock tunnel closed a switch to operate the solenoid valve, which opens the supply valve. As the fuel flowed to the model and fuel injection orifices, its pressure was monitored by a PCB piezoelectric pressure transducer. The system was designed so that sonic flow occurred at the orifices. As shown, the fuel tank and valve assembly was shielded from the flow by an aerodynamic shroud. In normal operation, the upstream end of this shroud was located 50 mm downstream of the termination of the scramjet afterbody, and to check that this was sufficient for the shroud to have no influence on the forces on the scramjet, a test was run with an insert to increase this distance to 125 mm. No change in the measured force was observed.

The pressure measured by the pressure sensor, together with calibration factors for the injection orifices were used to determine the mass flow rate of the fuel. This was varied by changing the filling pressure of the fuel tank. The stress bar was mounted horizontally, as in the previous tests.

(b) Measurements

The model employed here was larger and more complicated than the cones of the previous studies, so it was necessary to again check that the distribution of forces was not important. This was done numerically. A two dimensional axisymmetric finite element 70 x 6 mesh was made to represent the model and fuel tank, and three point loads were applied which approximately represented the loading on the model during a test. One represented the drag

of the model, and was applied at the nose, one represented thrust due to fuel injection, and was applied at the location of the injection orifices, and one represented the thrust due to mixing and combustion, and was applied at a point halfway along the thrust surface. The variation with time of each of these is shown in Figure 11(a). Together these three produced the strain gauge response shown in Figure 11(b). This was then deconvolved, using only the impulse response function g(t) for the load at the nose, to see if the applied time history of the force on the model could be recovered. The result is shown as the solid line in Figure 11(c), where it is compared with the sum of the three forces acting on the model. It can be seen that, apart from a time delay of about 100 μ sec, the deconvolved signal is in good agreement with the input signal, signifying that the measured value of force was independent of its distribution.

This also confirmed that the experimental method of determining g(t) could be used for this configuration.

A typical strain gauge output obtained when fuel is injected is shown in Figure 12. The operation of the solenoid valve was timed so that the fuel injection pressure began to rise approximately 5 milliseconds before initiation of the test flow, reached its test value approximately 0.5 milliseconds before flow initiation, and remained approximately constant for 3 milliseconds. The thrust due to fuel injection therefore begins some 3 milliseconds before the test flow, and this is evident on the strain gauge output. Then the flow starting processes and the fuel induced combustion produce larger forces, which lead to more rapid variations in the gauge output.

Records such that in Figure 12 were deconvolved using the experimentally determined g(t), leading to force time histories as shown in Figure 13. The test section pitot pressure and static pressure are presented in Figure 13(a), and display approximately steady conditions during the test time. Figure 13(b) shows three force histories. One is obtained when fuel is not injected and the test gas is air. Then the scramjet drag is 150 ± 20 N. Another is obtained when nitrogen is used as test gas and fuel is injected. Then the drag is approximately 50 N less than the fuel off test in air. There is a small difference in flow conditions between air and nitrogen test gases, however the drag reduction is due primarily to the injection of fuel. It can be seen that, prior to arrival of the test flow, fuel injection induces a thrust of approximately 30 N. The remaining 20 N reduction in drag possibly results from fuel/test gas flow interactions.

Finally, Figure 13(c) displays the result of injecting fuel with air test gas. Prior to the test flow fuel injection again induces a net thrust of 30 N. Then, as the flow over the model is established the drag increases, closely following the result obtained with nitrogen test gas. However, ignition of the fuel then causes thrust, which increases until it becomes quasi-steady at a net thrust of 60 ± 15 N. This, in conjunction with the other two time histories, clearly demonstrates that a steady state of thrust can be generated by a scramjet model in the test time of a shock tunnel, and that it can be measured.

(c) Results and Discussion

Measurements of the thrust/drag obtained over a range of stagnation enthalpies are presented in Figure 14. Because the stress wave balance was still under development, the model was conservatively sized, and so the dimensions were not sufficient to produce combustion of pure hydrogen at the chosen shock tunnel operating pressures (measurements showed P = 1 atm. which according to Figure 4, is too small to yield vigorous combustion). This was confirmed experimentally. Therefore Silane (SiH_4) was used as an ignition promoter, and the experiments were conducted with a fuel mixture of 13% SiH_4 and 87% H_2, injected at an equivalence ratio of 0.8.

The variation of the thrust with tunnel stagnation enthalpy, or with the computed test section velocity, is shown in Figure 14. It can be seen that although the net thrust is positive around stagnation enthalpies of 3 MJ/kg, it falls off rapidly with increasing stagnation enthalpy. This is largely due to the increase in pre-combustion temperature as the stagnation enthalpy is increased. An attempt was made to increase the maximum thrust measured by either increasing the amount of fuel injected, or by lowering the tunnel stagnation enthalpy. In both cases unsteadiness in the flow resulted, suggesting the onset of thermal choking.

In order to confirm that the flow in the combustors was supersonic when combustion was taking place, pitot and static pressures were measured at the downstream end of one of the ducts just upstream of the expansion caused by the upstream corner of the afterbody. At a

stagnation enthalpy of 3.3 MK/kg the ratio of the two was 4.1, yielding a Mach number of 1.75 ± 0.1.

The variation of the drag of the model in the absence of fuel injection is also shown, and it can be seen that this dominates the overall performance of the model. This is not surprising, as little attention was given to optimising the aerodynamics, both internal and external, of the model. With attention given to this aspect, a considerably improved overall performance may be expected.

6. Conclusion

The discussion centred on Figure 5 emphasised the importance of maximising the model size if scramjet propulsion of vehicles at flight velocities of 3 to 4 km/sec is to be studied experimentally. The model used in these studies was designed with the primary aim of testing the use of the stress wave force balance, so was less than the maximum size possible in the tunnel. In fact, the length of the portion on which force was measured was approximately 0.3 m, while the length of the model assembly which governed the operation of the stress wave balance included the fuel tank, and therefore was 0.7 m, It is therefore clear that scope exists for use of a larger model, in which the fuel tank is integrated into the model, and this may be expected to allow combustion of pure hydrogen fuel.

The results of the tests performed to date are encouraging. The fact that it was possible to produce a quasi-steady state involving positive net thrust on an integrated configuration, and that the thrust could be measured, implies that the prospects for development and testing of scramjet propulsion at high flight speeds are considerably enhanced by the use of shock tunnels.

Acknowledgments

The authors would like to express their appreciation of the support provided by the Australian Research Council, and through NASA grant NAGW-674.

References

1. Billig, F.S. "Research on Supersonic Combustion" J. Prop & Power, V9 pp499-514, Jul-Aug 1993.
2. Anderson, G.Y., Bencze, D.P. & Sanders, B.W. "Ground tests confirm the promise of hypersonic propulsion" Aerospace America V25, No.9, pp38-42. Sept. 1987.
3. Stalker, R.J. "Development of a Hypervelocity Wind Tunnel" Aeron. J. of Royal Aero Soc. V76, pp374-384. June 1972.
4. Stalker, R.J. & Morgan, R.G. "Supersonic Hydrogen Combustion with a Short Thrust Nozzle" Comb. and Flame V57, pp55-70 July 1984.
5. Paull, A. "Hypersonic Ignition and Thrust Production in a Scramjet" AIAA paper 93-2444. Presented at AIAA/SAE/ASME/ASEE 29th Joint Propulsion Conference. Monterey, CA. June 28-30. 1993.
6. Naumann, K.W., Ende, H., Mathieu, G. & George, A. "Millisecond Aerodynamic Force Measurement with Side-Jet Model in the ISL Shock Tunnel" AIAA Journal, V31, pp1068-1074, June 1993.
7. Sanderson, S.R. & Simmons, J.M. "Drag Balance for Hypervelocity Impulse Facilities" AIAA Journal, V29, pp2185-2191. Dec 1991.
8. Simmons, J.M., Daniel, W.J., Mee, D.J. & Tuttle, S.L. "Force Measurement in Hypervelocity Impulse Facilities" in New Trends in Instrumentation for Hypersonic Research (ed. A. Boutier), Kluwer Academic Publishers, Amsterdam 1993, pp285-294.
9. Porter, L.M., Mee, D.J. & Simmons, J.M. "Measuring the effect on Drag Produced by Nose Bluntness on a Cone in Hypervelocity Flow" Proc. 11th Australasian Fluid Mechanics Conference(ed. M. Davis and G. Walker), Univ. of Tasmania, Hobart, Australia, 14-18 Dec, 1992, pp287-290.

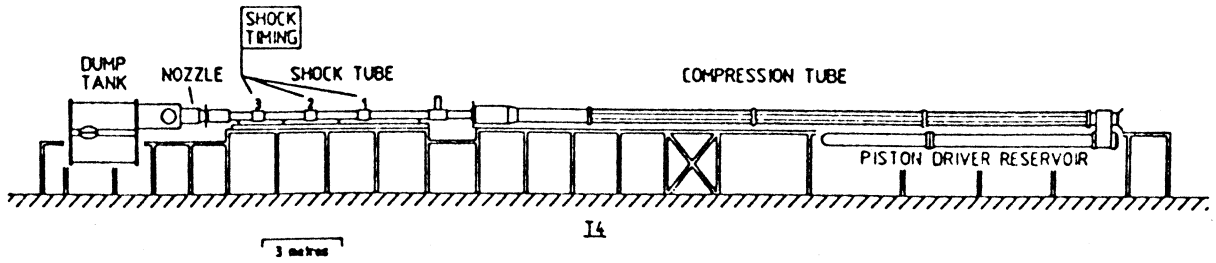

Fig. 1. Shock Tunnel T4

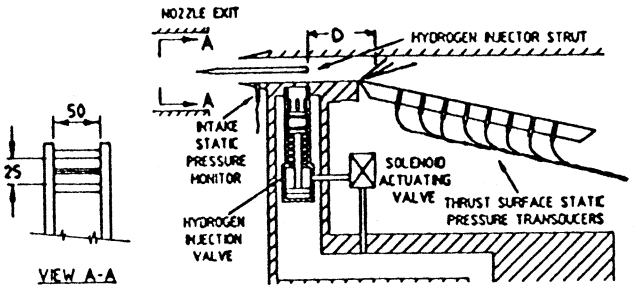

Fig. 2. Combustion Scaling Model

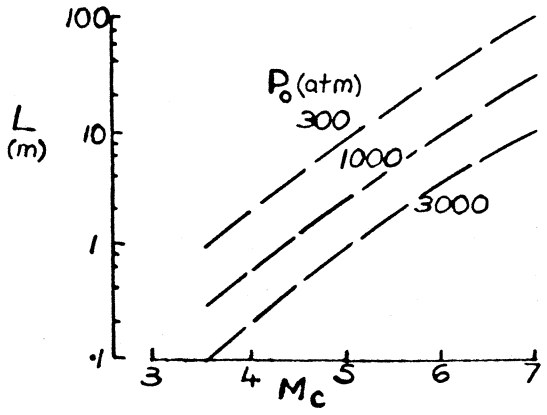

Fig. 5. Model Length

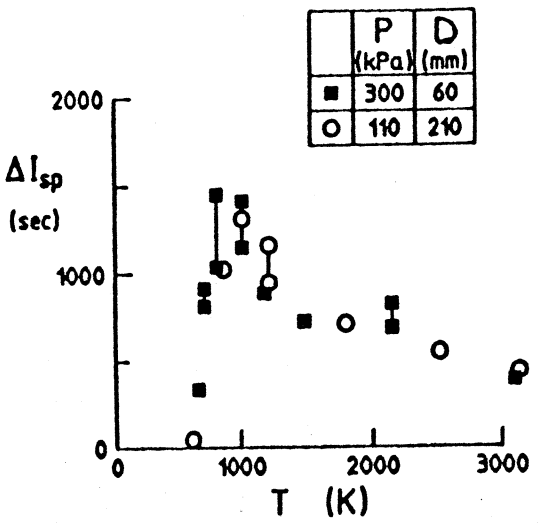

Fig. 3. Scaling of Combustion

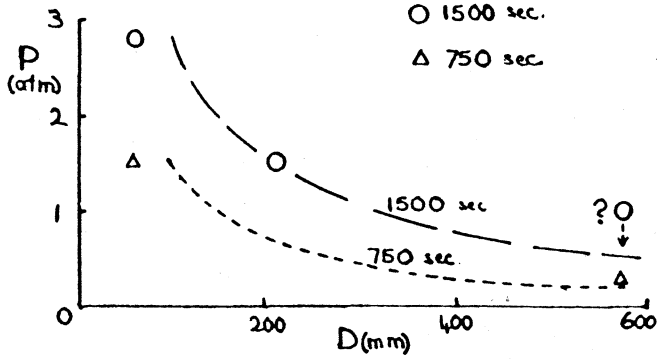

Fig. 4. Combustion Length for Thrust Generation

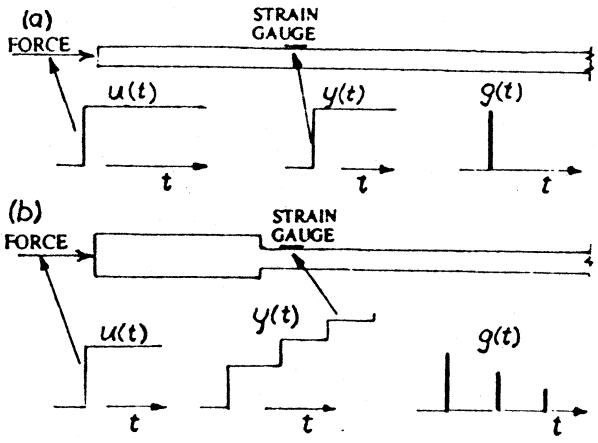

Fig. 6. Stress Wave Transmission

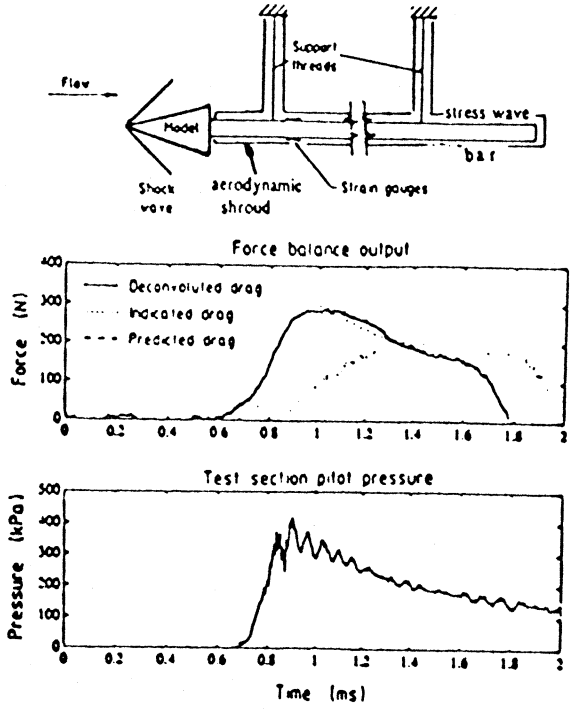

Fig. 7 Drag on 15° semi-vertex angle Cone H_0 = 4.0 MJ/kg, P_0 = 24 MPa

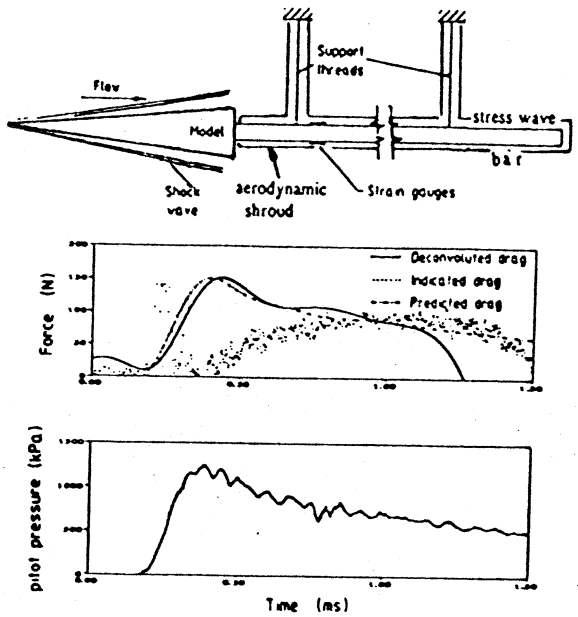

Fig. 8 Drag on 5° semi-vertex angle Cone H_0 = 7.8 MJ/kg, P_0 = 60 MPa

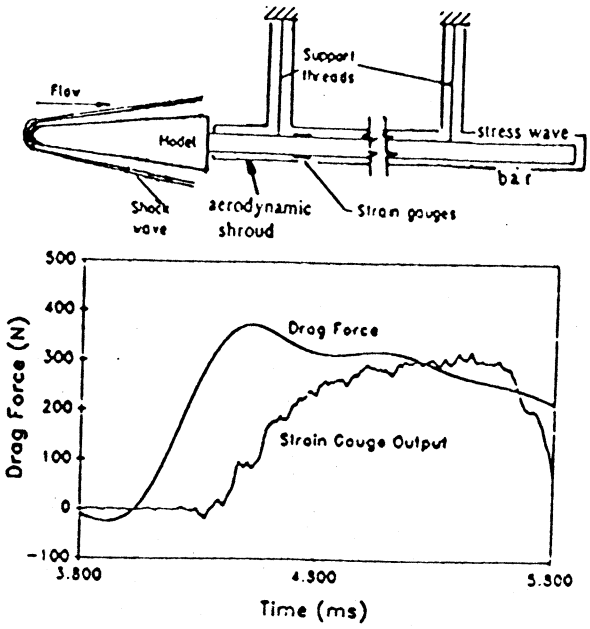

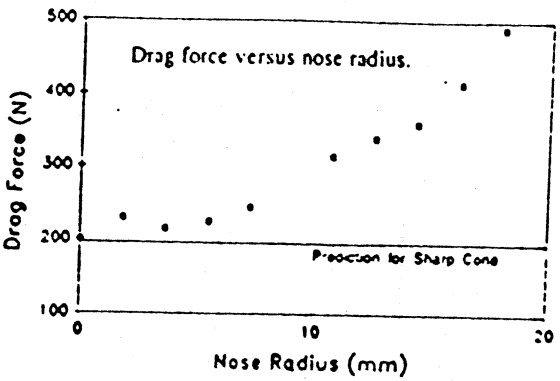

Fig. 9 Effect of nose blunting on drag of 5° semi-vertex angle Cone H_0 = 14.4 MJ/kg, P_0 = 38 MPa.

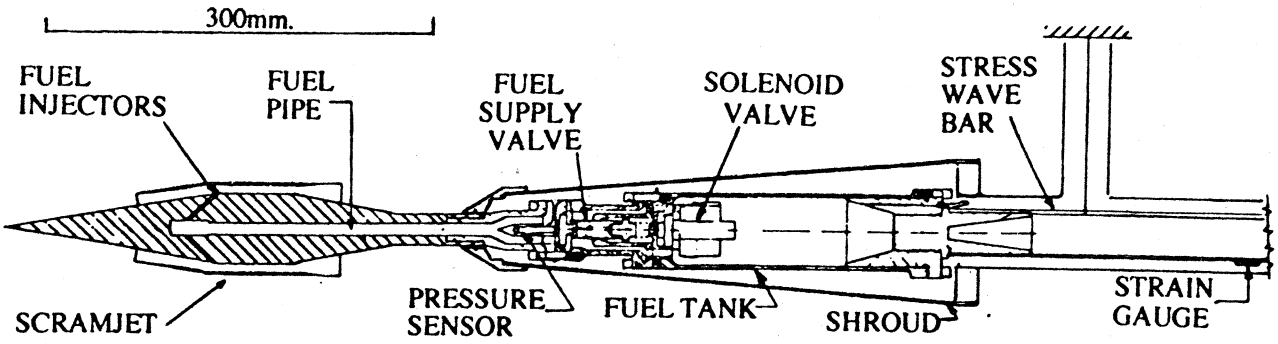

Fig. 10. Scramjet model and Fuel Tank Mounted on Stress Wave Bar

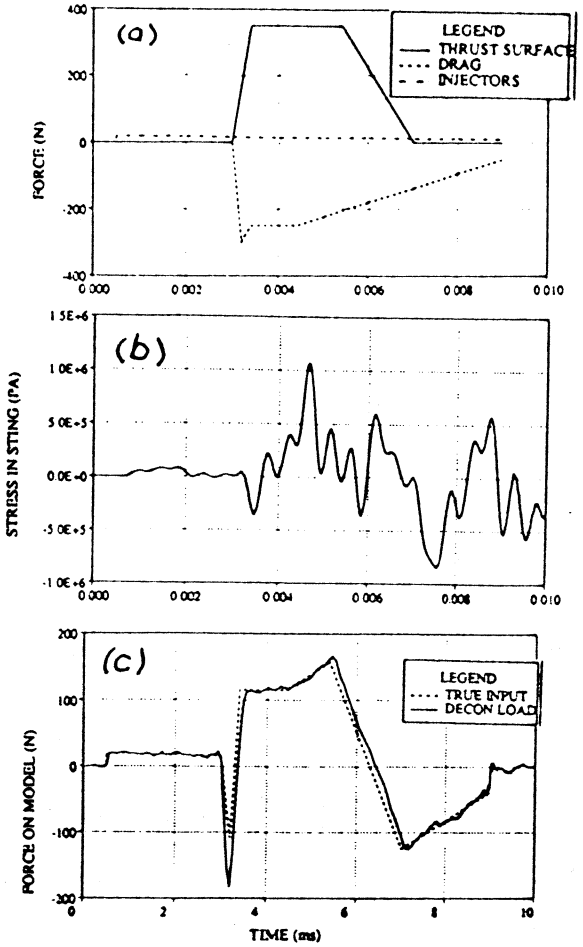

Fig. 11 Simulation of Distributed Load

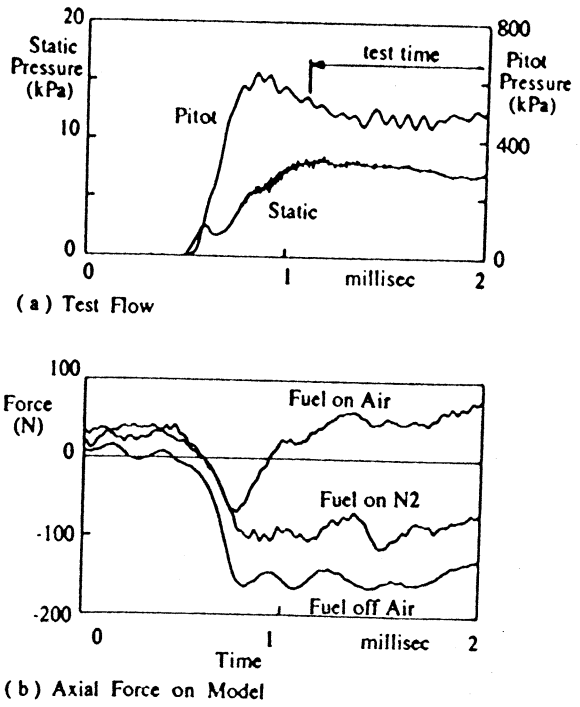

Fig. 13 Test Records showing generation of Net Thrust. H_0 = 3.2 MJ/kg; P_0 = 37 MPa.

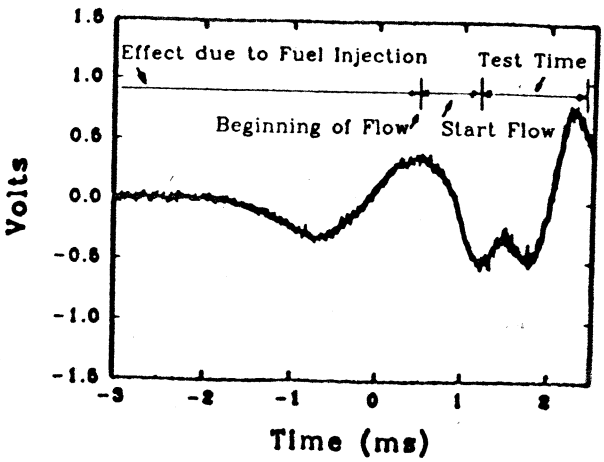

Fig. 12 Typical strain gauge output for Scramjet Tests.

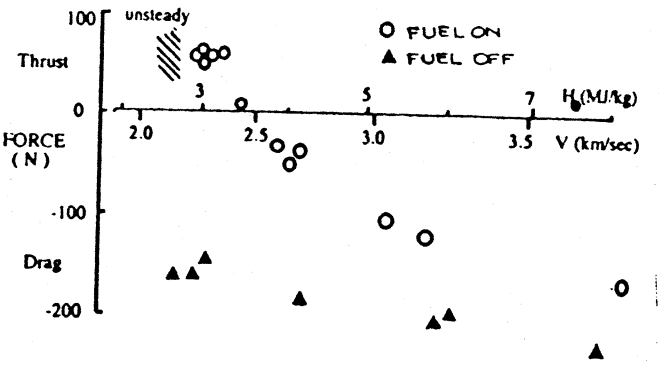

Fig. 14 Scramjet Thrust Measurements. P_0 = 37 ± 2.5 MPa, ϕ = 0.8.